

Middle East Respiratory Syndrome Coronavirus Infection Mediated by the Transmembrane Serine Protease TMPRSS2

Kazuya Shirato, Miyuki Kawase, Shutoku Matsuyama

Department of Virology III, National Institute of Infectious Diseases, Murayama Branch, Musashi-Murayama, Tokyo, Japan

The Middle East respiratory syndrome coronavirus (MERS-CoV) utilizes host proteases for virus entry into lung cells. In the current study, Vero cells constitutively expressing type II transmembrane serine protease (Vero-TMPRSS2 cells) showed larger syncytia at 18 h after infection with MERS-CoV than after infection with other coronaviruses. Furthermore, the susceptibility of Vero-TMPRSS2 cells to MERS-CoV was 100-fold higher than that of non-TMPRSS2-expressing parental Vero cells. The serine protease inhibitor camostat, which inhibits TMPRSS2 activity, completely blocked syncytium formation but only partially blocked virus entry into Vero-TMPRSS2 cells. Importantly, the coronavirus is thought to enter cells via two distinct pathways, one mediated by TMPRSS2 at the cell surface and the other mediated by cathepsin L in the endosome. Simultaneous treatment with inhibitors of cathepsin L and TMPRSS2 completely blocked virus entry into Vero-TMPRSS2 cells, indicating that MERS-CoV employs both the cell surface and the endosomal pathway to infect Vero-TMPRSS2 cells. In contrast, a single camostat treatment suppressed MERS-CoV entry into human bronchial submucosal gland-derived Calu-3 cells by 10-fold and virus growth by 270-fold, although treatment with both camostat and (23,25)-*trans*-epoxysuccinyl-L-leucylamido-3-methylbutane ethyl ester, a cathepsin inhibitor, or treatment with leupeptin, an inhibitor of cysteine, serine, and threonine peptidases, was no more efficacious than treatment with camostat alone. Further, these inhibitors were not efficacious against MERS-CoV infection of MRC-5 and WI-38 cells, which were derived from lung, but these characters differed from those of mature pneumocytes. These results suggest that a single treatment with camostat is sufficient to block MERS-CoV entry into a well-differentiated lung-derived cell line.

The isolation of a novel human betacoronavirus was first accomplished in Jeddah, Saudi Arabia, from a sputum specimen collected from a patient at 1 day after hospital admission. The virus was propagated by using African green monkey and rhesus macaque kidney epithelial cells (Vero and LLC-MK2 cell lines, respectively) and was termed the human betacoronavirus EMC/2012 (HCoV-EMC) (1). Recently, this virus was renamed the Middle East respiratory syndrome coronavirus (MERS-CoV) (2). Isolation of the virus from five subsequently identified patients was successful. Furthermore, the entire genomic sequence of MERS-CoV was elucidated from viral RNA in the sputum specimens (3). Thereafter, a number of cell lines susceptible to MERS-CoV were reported (4), including the human-derived Calu-3, HFL, Caco-2, Huh-7, HEK, and His-1 cell lines. All of these cell lines exhibited cytopathic effects within a few days after MERS-CoV infection.

Next, the factors critical for MERS-CoV entry into cells were identified, including dipeptidyl peptidase 4 (DPP4) as a functional virus receptor (5) and certain cellular proteases (e.g., type II transmembrane serine protease [TMPRSS2] and members of the cathepsin family) as activators of the viral spike (S) glycoprotein (6). The protease inhibitors camostat and MDL28170 efficiently inhibit entry of pseudotyped MERS-CoV into the human colorectal cell line Caco-2 (6), lending support to the role of cellular proteases in virus entry into cells.

Similar to the severe acute respiratory syndrome coronavirus (SARS-CoV), cellular protease availability to MERS-CoV is thought to determine its entry route into host cells. In the absence of proteases at the cell surface, MERS-CoV reportedly enters cells by a cathepsin-mediated endosomal pathway. On the other hand, in the presence of proteases (e.g., TMPRSS2) on the cell surface, MERS-CoV can apparently enter cells either at the cell surface or

via the early endosome (6). Therefore, TMPRSS2-expressing cells in the lung may provide an initial site of coronavirus infection. On the basis of the activation of SARS-CoV and mouse hepatitis virus strain 2 (MHV-2) S proteins, a two-step conformational change seems to be necessary for the induction of membrane fusion (7, 8). The first step takes place after binding of the virus to its cell surface receptor, and the second step is driven by the cleavage of the viral S protein by cellular proteases.

TMPRSS2 is expressed in the epithelial cells of the human respiratory and gastrointestinal tracts (9), and its ability to activate viral glycoproteins has been reported for influenza A virus, metapneumovirus, and the coronaviruses (6, 9–22). We previously showed that TMPRSS2 enhances virus replication and syncytium formation during infection by SARS-CoV, HCoV-NL63, and the porcine epidemic diarrhea virus, increasing virus entry into host cells (19, 22) or virus release from the cell surface (21). SARS-CoV infection in particular leads to syncytium formation in TMPRSS2-expressing cells. Therefore, the current study explored the role of TMPRSS2 in MERS-CoV infection by using Vero-TMPRSS2 cells. Furthermore, we assessed the ability of camostat and other protease inhibitors to block virus infection by using Calu-3 human bronchial epithelial cells.

Received 10 July 2013 Accepted 6 September 2013

Published ahead of print 11 September 2013

Address correspondence to Shutoku Matsuyama, matuyama@nih.go.jp.

Copyright © 2013, American Society for Microbiology. All Rights Reserved.

doi:10.1128/JVI.01890-13

TABLE 1 Primers and probes employed for real-time PCR

Target mRNA (method of detection)	Primer or probe	
	Name ^a	Sequence
MERS-CoV-N (hybridization) for virus cell entry assay	EMC-Leader	CTCGTTCTCTTGCAGAACTTTG
	EMC-R	TGCCCAGGTGGAAGGT
	EMC-FITC	AGCCCAGTGTACCAAGAGACAGTGTATTG
	EMC-LC	TGCAGCTCGTGGTTTTGGATTACGTCTT
MERS-CoV-upE (TaqMan) for multistep growth assay	upE-F	GCAACGCGCATTTCAGTT
	upE-R	GCCTCTACACGGGACCCATA
	upE-FAM	CTCTTCACATAATCGCCCCGAGCTCG
HCoV-229E-N (TaqMan) for virus cell entry assay	229E-Leader	GAAAAGTTGCTTTTTAGACTTTGTGTCTA
	229E-R	GGTATCACCTTCCAAGATTGTTC
	229E-FAM	GCATCTGAACCACAACG
Human DPP4 (hybridization)	DPP4-F	TGACATGGGCAACAAGA
	DPP4-R	AACCCAGCCAGTAGTACTC
	DPP4-FITC	GGTCATGGATATTTGTGACTATGATGAATCCAGTGG
	DPP4-LC	AGATGGAACGTCTTAGTGCCACGG
Human TMPRSS2 (hybridization)	TMPRSS2-F	CTCTACGGACCAAACCTTCATC
	TMPRSS2-R	CCACTATTCTTGGCTAGAGTA
	TMPRSS2-FITC	TCAGAGGAAGTCTGGCACCCTGTGTG
	TMPRSS2-LC	CAAGACGACTGGAACGAGAACTACGGGC
Human HAT (hybridization)	HAT-F	CTTGTGAGACTTGAGAACAGTG
	HAT-R	ACCTGTCCCTGCCTTAGC
	HAT-FITC	GCCAGCATATTCTTGAGCGCCCA
	HAT-LC	CCTGTTACATAAGCAGTAGAGCCAGGTGGAAT
Human cathepsin L (SYBR)	CatL-F	GTGGACATCCCTAAGCAGGA
	CatL-R	CACAATGGTTTCTCCGGTC
Human SP-D (TaqMan)	SP-D_F	TCCAGGCTGCTTTCTCTCAG
	SP-D_R	TTGAAAATCTTCTCCCGACA
	SP-D_FAM	AAAGTTGAGCTTCTCCCAAATGGCCA
Human GAPDH (TaqMan)	GAPDH_F	GAAGGTGAAGGTCGGAGTCAAC
	GAPDH_R	CAGAGTTAAAAGCAGCCCTGGT
	GAPDH_FAM	TTTGTCGTATTGGGCGCCT

^a R, reverse; FITC, fluorescein isothiocyanate; LC, LC Red 640; F, forward; FAM, 6-carboxyfluorescein.

MATERIALS AND METHODS

Cells and viruses. HeLa cells, HeLa cells constitutively expressing TMPRSS2 (HeLa-TMPRSS2 cells), Vero cells, and Vero cells constitutively expressing TMPRSS2 (Vero-TMPRSS2 cells) were grown in Dulbecco's modified Eagle's medium (DMEM; Nissui) supplemented with 5% fetal bovine serum (Gibco-BRL). MERS-CoV (provided by Ron A. M. Fouchier, Erasmus Medical Center, Rotterdam, The Netherlands) and SARS-CoV Frankfurt 1 (provided by John Ziebuhr, University of Würzburg, Würzburg, Germany) were propagated by using Vero cells or Vero-E6 cells and assayed according to the 50% tissue culture infectious dose (TCID₅₀) method. Human lung-derived WI-38, MRC-5, and Calu-3 cell lines were cultured as recommended by the American Type Culture Collection.

Proteases and inhibitors. The following proteases were used in this study: trypsin (catalog no. T8802; Sigma), chymotrypsin (catalog no. C3142; Sigma), elastase (catalog no. E0258; Sigma), thermolysin (catalog no. P1512; Sigma), endoproteinase Arg-C (catalog no. P6056; Sigma), and endoproteinase Lys-C (catalog no. P3428; Sigma). All proteases were dissolved in DMEM and used at the concentrations indicated in the appropriate figure legends. In addition, the following inhibitors were used: EST [(23,25)-*trans*-epoxysuccinyl-L-leucylamido-3-methylbutane ethyl es-

ter; catalog no. 330005; Calbiochem], bafilomycin A1 (catalog no. B1793; Sigma), cathepsin L inhibitor III (catalog no. 219427; Calbiochem), cathepsin B inhibitor CA-074 (catalog no. C5857; Sigma), cathepsin K inhibitor II (Z-L-NHNHCONHNH-LF-Boc; catalog no. 219379; Calbiochem), cathepsin S inhibitor (Z-FL-Cocho; catalog no. 219393; Calbiochem), leupeptin (product no. 11017101001; Roche), and camostat mesylate (catalog no. 3193; Tocris Bioscience). The inhibitors were used at the concentrations indicated in the appropriate figure legends.

Cell entry assay for authentic MERS-CoV. Confluent HeLa, HeLa-TMPRSS2, Vero, Vero-TMPRSS2, MRC-5, WI-38, and Calu-3 cells in 96-well plates were pretreated with inhibitors for 30 min. Cells were then inoculated with MERS-CoV (10⁴ TCID₅₀) and incubated with the inhibitors for 1 h at 37°C, followed by culture at 37°C for 5 h. Cellular RNA was isolated by the addition of Isogen reagent (100 µl; Nippon Gene). A real-time PCR assay was performed to ascertain the amount of newly synthesized subgenomic MERS-CoV RNA by using the primers and probes listed in Table 1. PCR analysis was performed by using a LightCycler-Nano instrument (Roche Diagnostics), as described previously (23).

Western blot analysis. Preparation of cell lysates, sodium dodecyl sulfate-polyacrylamide electrophoresis (SDS-PAGE), and electrical transfer of proteins onto nitrocellulose transfer membranes were described

previously (8, 22). The viral S protein was detected by using an antipeptide antibody against the very highly conserved region (VHCR; corresponding to the amino acid sequence TGRSAIEDVLFDKVK) of the MHV-2 spike protein, glyceraldehyde 3-phosphate dehydrogenase (GAPDH) was detected by reaction with an anti-GAPDH antibody (catalog no. IMG-5143A; Imgenex), and DPP4 was detected by reaction with an anti-CD26 antibody (ab129060; Abcam). Bound primary antibodies were then reacted with a horseradish peroxidase-conjugated secondary anti-rabbit IgG (anti-R-IgG; catalog no. ALI3404; Biosource International). Immunoreactive bands were visualized by using an enhanced chemiluminescence kit (ECL-plus; Amersham Pharmacia) and an LAS-3000 instrument (Fuji).

Sucrose density gradient centrifugation. Culture fluid collected from MERS-CoV-infected cells was centrifuged for 10 min at 3,000 rpm. Then, 7 ml of the supernatant was overlaid onto a sucrose gradient consisting of 3 ml of 20% sucrose and 3 ml of 60% sucrose in a 13-ml Ultra-Clear centrifuge tube (Beckman). After centrifugation at 28,000 rpm for 1 h at 4°C, 1-ml fractions were drawn from the air-fluid interface, the fluid–20% sucrose interface, and the 20% sucrose–60% sucrose interface. The sucrose in the samples was replaced with phosphate-buffered saline using a centrifugal filter (Amicon Ultra 100K; Millipore). The samples were then subjected to Western blot analysis as described above.

FFWO assay. The fusion-from-without (FFWO) assay was performed as previously described (24). Briefly, Vero-TMPRSS2 cells in 96-well plates were inoculated with a high titer (10^6 PFU) or a low titer (10 PFU) of authentic MERS-CoV diluted in DMEM. Cells were incubated with virus on ice for 1 h. The cell culture medium was replaced with fresh medium prewarmed to 37°C in the presence or absence of 100 µg/ml cycloheximide. After incubation for 3, 5, or 20 h, the cells were fixed with 4% formaldehyde and stained with crystal violet.

Multistep growth of MERS-CoV. Confluent MRC-5, WI-38, and Calu-3 cells in 24-well plates were cultured for 7 days, inoculated with MERS-CoV (10 PFU), and incubated for 2 h at 37°C. Residual virus was removed, and fresh medium containing camostat at the indicated concentrations was added to the cells. Total RNA was isolated from the virus-containing conditioned medium collected from each of four wells at seven 24-h intervals by using Isogen-LS reagent (Nippon Gene). Real-time PCR was performed to estimate viral growth kinetics, as previously described (22). The primers and probes used to quantify viral RNA replication are described in Table 1.

Quantification of transcripts in lung-derived cell lines. Total cellular RNA was isolated from WI-38, MRC-5, Calu-3, Vero, and HeLa cells by using the Isogen reagent. Real-time PCR was performed to quantify mRNA expression levels of DPP4, human airway trypsin-like protease (HAT), TMPRSS2, cathepsin L, surfactant protein D (SP-D), and GAPDH. The mRNA expression levels in these cells were compared with the expression levels in total human lung RNA isolated from three male and three female Caucasian individuals, aged 32 to 61 years (catalog no. 636524; purchased from Clontech). Primers and probes for real-time PCR are described in Table 1. Real-time PCR analysis was performed by using a LightCycler-Nano instrument. The comparative expression of mRNA in each cell sample was calculated on the basis of a calibration line obtained by 10-fold stepwise dilution of human lung RNA.

RESULTS

Syncytium formation in MERS-CoV-infected Vero cells in the presence of exogenous proteases. We employed authentic MERS-CoV to assess protease-inducible syncytium formation in Vero cells. Vero cells were infected with MERS-CoV at a multiplicity of infection (MOI) of 0.01, incubated for 15 h, and then treated with a variety of proteases for 6 h. Trypsin, chymotrypsin, elastase, and thermolysin all induced the formation of large syncytia (Fig. 1). Endoprotease Lys-C, which specifically cleaves proteins at the carboxyl side of lysine residues, also induced syncytium formation, but endoprotease Arg-C, which specifically

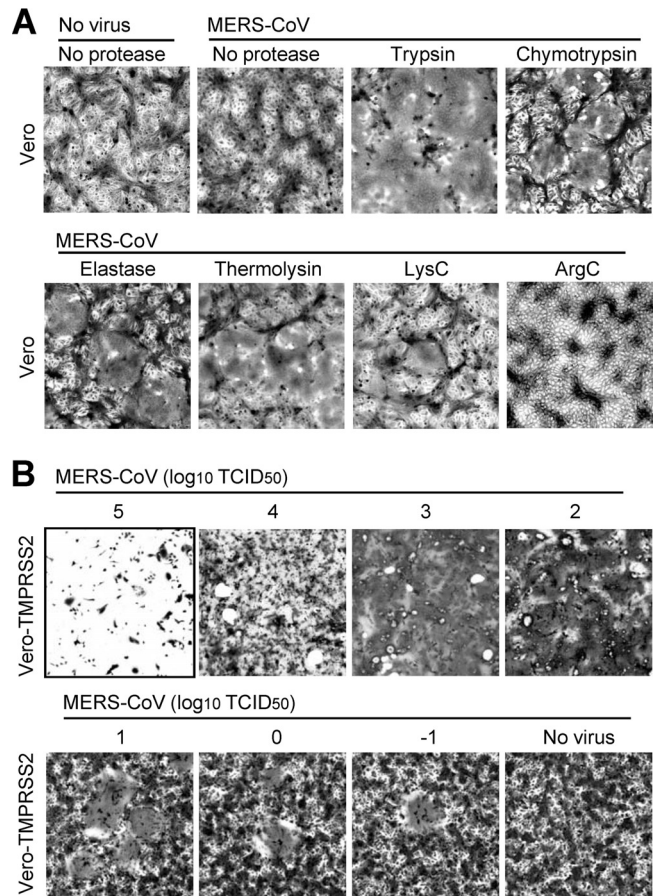


FIG 1 Syncytium formation induced by proteases in Vero cells infected with MERS-CoV. (A) Vero cells infected with MERS-CoV at an MOI of 0.01 were cultured for 15 h and then treated for 6 h with a variety of proteases, trypsin (1 µg/ml), chymotrypsin (10 µg/ml), elastase (10 µg/ml), thermolysin (1 µg/ml), endoprotease Arg-C (20 µg/ml), or endoprotease Lys-C (20 µg/ml). (B) Vero-TMPRSS2 cells were infected with serially diluted MERS-CoV in the absence of exogenous proteases and incubated for 18 h. Cells were fixed with formaldehyde and stained with crystal violet.

cleaves proteins at the carboxyl side of arginine residues, did not. This result indicates that the lysine residues at the cleavage site in the viral S protein are a target for trypsin. The syncytia were more pronounced in Vero cells that constitutively expressed type II transmembrane serine protease TMPRSS2 (Vero-TMPRSS2 cells) than in the exogenous protease-treated parental Vero cells. The Vero-TMPRSS2 cells were inoculated with 10-fold serially diluted MERS-CoV at an MOI of 10 ($5 \log_{10}$ TCID₅₀s) and incubated for 18 h. Figure 1B shows cell debris at $5 \log_{10}$ TCID₅₀s, whereas almost all of the cells were fused at 4 to $2 \log_{10}$ TCID₅₀s. Large syncytium formation was clearly observed at $<1 \log_{10}$ TCID₅₀. No cytopathic effects were observed in parental Vero cells at 18 h postinfection (data not shown).

Susceptibility of TMPRSS2-expressing cells to MERS-CoV. Vero and Vero-TMPRSS2 cells were assessed for their susceptibility to MERS-CoV. First, virus stocks of MERS-CoV and SARS-CoV were titrated for infectivity in both cell types by the TCID₅₀ method (Table 2). The titer of SARS-CoV in Vero-TMPRSS2 cells tended to be higher than that in Vero cells (7.2 ± 0.5 versus $6.3 \pm 0.5 \log_{10}$ TCID₅₀s). In contrast, the titer of MERS-CoV in Vero-

TABLE 2 Susceptibility of Vero-TMPRSS2 cells to MERS-CoV and SARS-CoV

Virus	Cell type	Susceptibility (log ₁₀ TCID ₅₀)	Virus production (log ₁₀ TCID ₅₀)	
			Inoculated virus	Propagated virus
MERS-CoV	Vero	4.3 ± 0.5	5	5.0 ± 0.7
			4	4.3 ± 0.4
			3	3.5 ± 0.5
			2	2.3 ± 0.4
			1	2.5 ± 0.5
	Vero-TMPRSS2	6.3 ± 0.5	5	7.0 ± 1.5
			4	5.5 ± 1.1
			3	5.5 ± 0.5
			2	4.8 ± 0.4
			1	3.8 ± 0.4
SARS-CoV	Vero	6.3 ± 0.5	5	5.7 ± 0.3
			4	5.5 ± 0.5
			3	5.5 ± 0.5
			2	4.8 ± 0.4
			1	3.8 ± 0.4
	Vero-TMPRSS2	7.2 ± 0.5	5	6.1 ± 0.2
			4	5.5 ± 1.1
			3	5.5 ± 0.5
			2	4.8 ± 0.4
			1	3.8 ± 0.4

TMPRSS2 cells was 100-fold higher than that in Vero cells (6.3 ± 0.5 versus 4.3 ± 0.5 log₁₀ TCID₅₀s).

Next, MERS-CoV growth in Vero and Vero-TMPRSS2 cells was investigated. Aliquots of the culture medium were collected from the cells shown in Fig. 1B, in which Vero-TMPRSS2 cells were inoculated with serially diluted MERS-CoV and incubated for 18 h. The collected culture medium was then used for titration. For each virus dilution, the virus titer in the Vero-TMPRSS2 cell medium was 1 or 2 log units higher than that in the parental Vero cell medium (Table 2). In comparison, SARS-CoV did not induce large syncytia in Vero-TMPRSS2 cells, and therefore, the medium could be collected without prominent cell death at 48 h after infection. The growth of both MERS-CoV and SARS-CoV did not differ significantly between the two cell types, as illustrated in Table 2.

Western blot analysis of viral S protein. Next, the culture media and cell lysates from the virus-infected Vero cells or the virus-infected Vero-TMPRSS2 cells shown in Fig. 1B were collected and subjected to Western blot analysis. Western blotting was performed using an antipeptide antibody that recognizes the VHCR of the MHV-2 S2 subunit. MHV-2 VHCR corresponds to amino acid sequence TGRSAIEDVLFDKVK, which is similar to the same region in the MERS-CoV S protein, SARSAIEDLLFDKVT. Figure 2 shows that a 180-kDa MERS-CoV S protein was detected in the culture medium of parental Vero cells after infection with 5 log₁₀ TCID₅₀s and in the culture medium of Vero-TMPRSS2 cells after infection with 5, 4, and 3 log₁₀ TCID₅₀s. The anti-VHCR peptide antibody also reacted with 180-kDa and 120-kDa bands in the cell lysates of both cell types. The 120-kDa S protein was not observed in the culture fluid (Fig. 2, Medium) or in the virus purified by sucrose gradient centrifugation (Fig. 3). We hypothesize that the 180-kDa band corresponds to the intact viral S protein and that the 120-kDa band is a degradation product of the S protein.

The 180-kDa band was more pronounced in both the cell lysate and the culture medium of Vero-TMPRSS2 cells at 4 and 3 log₁₀ TCID₅₀s than at 5 log₁₀ TCID₅₀s. In all likelihood, the dramatic

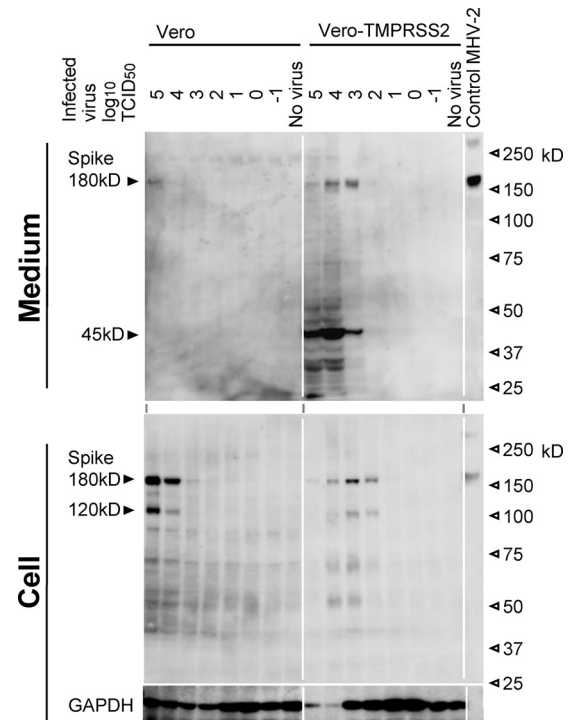


FIG 2 Western blot analysis of the MERS-CoV S protein. Culture medium samples and cell lysates were collected from parental Vero cells or Vero-TMPRSS2 cells at 18 h after infection with MERS-CoV. Samples were subjected to SDS-PAGE (3 to 10% gradient gel) and transferred to a nitrocellulose membrane. The viral S protein was detected by using an antipeptide antibody against the VHCR of the MHV-2 S protein, followed by a horseradish peroxidase-conjugated anti-rabbit IgG. MHV-2 was used as the positive control for the anti-VHCR antibody. GAPDH was used as the loading control and was detected by using an anti-GAPDH antibody.

membrane fusion induced by MERS-CoV in Vero-TMPRSS2 cells caused cytotoxicity at higher titers, thereby reducing S-protein production. Furthermore, larger amounts of the viral S protein were observed in the cell lysate than in the culture medium of

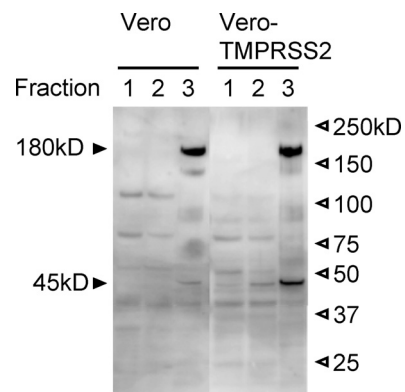


FIG 3 Incorporation of the 45-kDa S protein into virus particles. Culture medium collected from Vero-TMPRSS2 cells at 18 h after infection with 4 log₁₀ TCID₅₀s of MERS-CoV was overlaid onto the top fraction of a sucrose step gradient (20% and 60%) and centrifuged at 28,000 rpm for 1 h. The fractions were drawn from the air-fluid interface (fraction 1), the fluid–20% sucrose interface (fraction 2) and the 20% sucrose–60% sucrose interface (fraction 3) and subjected to Western blot analysis (3 to 10% gradient gel). The viral S protein was detected as described in the legend to Fig. 2.

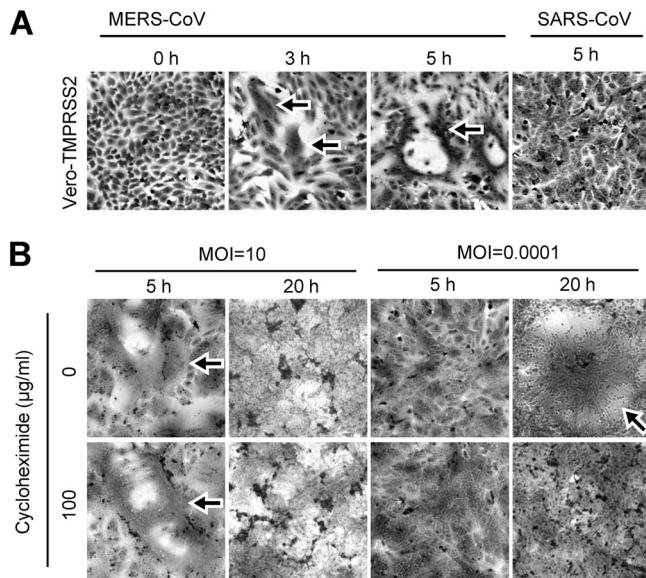


FIG 4 Induction of fusion from without by MERS-CoV particles. (A) A high-titer sample (MOI = 10) of MERS-CoV or SARS-CoV was adsorbed onto Vero-TMPRSS2 cells on ice for 1 h. The culture medium was then exchanged for fresh, prewarmed medium (37°C). Cells were incubated for 3 or 5 h, fixed, and stained with crystal violet. (B) Vero-TMPRSS2 cells were inoculated with MERS-CoV at a high titer (MOI = 10) or a low titer (MOI = 0.0001) for 1 h on ice and then shifted to 37°C in the presence or absence of cycloheximide (100 µg/ml). Cells were incubated for 5 or 20 h, fixed, and stained with crystal violet. Arrows, fused cells.

parental Vero cells. Vero-TMPRSS2 cells, on the other hand, displayed reduced amounts of viral S protein in the cell lysate compared with Vero cells but secreted more S protein into the medium. Interestingly, a 45-kDa degradation product was also observed in the culture medium of Vero-TMPRSS2 cells at 5, 4, and 3 log₁₀ TCID₅₀s, in parallel with the production of the 180-kDa S protein. However, this 45-kDa band was not observed in the corresponding cell lysates. These results imply that TMPRSS2-mediated cleavage of the viral S protein at the S2 subunit generates the 45-kDa band, thereby enhancing virus release from the cell by an unknown mechanism. To confirm the incorporation of the 45-kDa S protein into the virus particle, the virus was purified by sucrose density gradient centrifugation, as described in Materials and Methods. The 45-kDa band was observed with the 180-kDa band at the 20% sucrose–60% sucrose interface, which is where the virus particle is predicted to centrifuge to (Fig. 3).

Virus particle-induced cell-cell fusion. To confirm the ability of the MERS-CoV S protein to induce cell-cell fusion in Vero-TMPRSS2 cells, we carried out a FFWO assay. Briefly, a high titer (MOI = 10) or a low titer (MOI = 0.0001) of MERS-CoV was adsorbed onto Vero-TMPRSS2 cells on ice for 1 h. The cells were then shifted to 37°C in the presence or absence of cycloheximide (100 µg/ml), an inhibitor of protein translation. In the high-titer-virus-inoculated cells, a barely detectable level of cell-cell fusion was observed at 3 h postinfection, the level increased at 5 h (Fig. 4A), and fusion affected all of the cells by 20 h (Fig. 4B). No cell-cell fusion was observed in SARS-CoV-infected cells at 5 h postinfection (Fig. 4A). Cell-cell fusion was not inhibited by cycloheximide, although cell fusion induced by the newly synthesized viral S protein (fusion from within) was completely blocked

for 20 h following low-titer infection (Fig. 4B). These results indicate that the S protein on the MERS-CoV particle is sufficient for the induction of cell-cell fusion in the absence of protein synthesis.

Inhibition of syncytium formation by camostat. We next employed camostat mesylate, an inhibitor of TMPRSS2 activity (22), to confirm the proteolytic activation of syncytium formation by TMPRSS2. Vero-TMPRSS2 cells were infected with MERS-CoV at an MOI of 0.0001. The cells were then cultured in the presence of serially diluted camostat. Cells were stained with crystal violet, and the extent of syncytium formation was quantified by counting the number of nuclei in the fused cells ($n = 8$ syncytia). Syncytia were observed in the absence of camostat at 15 h postinfection, but camostat blocked their formation (Fig. 5A). Syncytium formation was moderately inhibited by camostat at concentrations of 1 µM and 10 µM and completely inhibited at 100 µM (Fig. 5B). Thus, camostat can prevent syncytium formation by inhibiting TMPRSS2.

Next, Western blot analysis of the cell lysate and the medium was conducted using the anti-VHCR peptide antibody to detect inhibition of TMPRSS2 cleavage of the viral S protein. In cell lysates, the 180- and 120-kDa S-protein bands were observed; however, inhibition of cleavage to explain the cell-cell fusion inhibition by camostat was not observed (Fig. 5C). In the culture medium, the production of the 45-kDa fragment was clearly inhibited by the addition of camostat, indicating that the 45-kDa fragment is produced by TMPRSS2.

Inhibition of virus entry into cells by protease inhibitors. To clarify the mechanism underlying the high susceptibility of Vero-TMPRSS2 cells to MERS-CoV infection, virus entry into the cells was assessed by real-time PCR, as described previously for SARS-CoV and HCoV-NL63 (22). Unsusceptible HeLa cells served as the negative control. MERS-CoV entry into Vero-TMPRSS2 cells was ~20-fold higher than that into Vero cells, while supplemental trypsin in the culture medium enhanced virus entry into Vero cells by only 5-fold (Fig. 6A). Camostat (10 µM) impaired MERS-CoV entry by 15-fold, whereas only slight inhibition (~3-fold decrease) was obtained with 10 µM EST, an inhibitor of endosomal cathepsins (Fig. 6B). Furthermore, camostat inhibited virus infection in Vero-TMPRSS2 cells, but not in Vero cells. This indicates that the drug specifically inhibited the TMPRSS2 utilized by MERS-CoV for cell entry. Given that the EST concentration in this experiment was sufficient to inhibit MERS-CoV infection in TMPRSS2-negative cells, these results suggest that large populations of virus utilize cell surface TMPRSS2, when available for cell entry, rather than resident endosome cathepsins.

Simultaneous treatment with camostat and EST dramatically blocked virus infection (~180-fold decrease) in Vero-TMPRSS2 cells, indicating that MERS-CoV can enter the cells via two distinct pathways, the cell surface pathway and the endosomal pathway. This observation is consistent with that from an earlier study regarding SARS-CoV entry into cells (22) and also supports previous results obtained with pseudotyped MERS-CoV and Caco-2 cells (6).

Next, we confirmed which endosomal cathepsins are employed by MERS-CoV for cell entry by using inhibitors against cathepsins B, L, K, and S in TMPRSS2-negative Vero cells. MERS-CoV cell entry was inhibited by ~40-fold by cathepsin L and cathepsin K inhibitors, but no significant suppression was observed by treatment with the cathepsin B or the cathepsin S inhibitor (Fig. 6C). Because the cathepsin K inhibitor also inhibits cathepsin

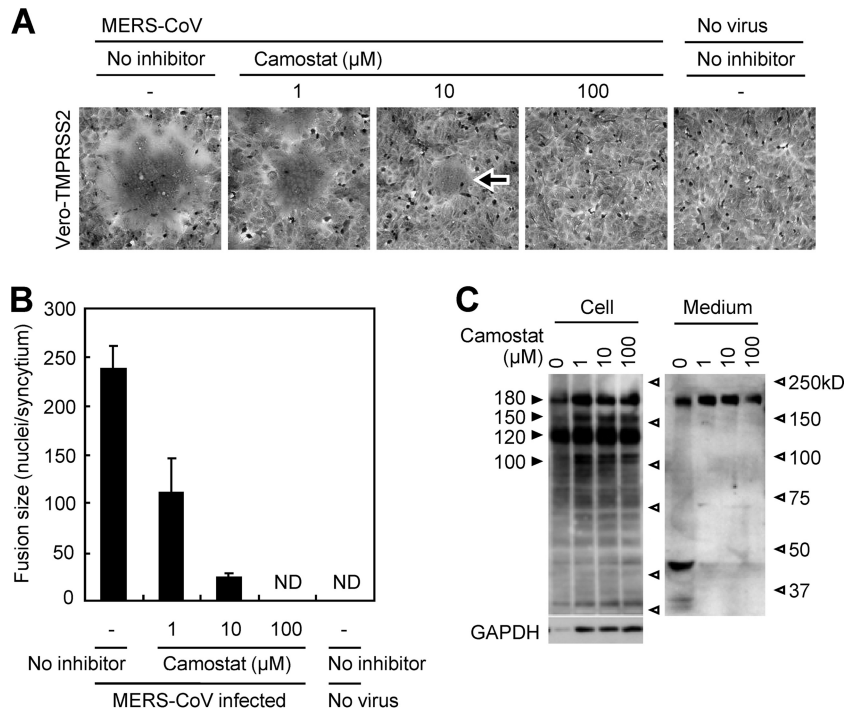


FIG 5 Inhibition of syncytium formation and S-protein degradation by camostat. (A) Vero-TMPRSS2 cells were infected with MERS-CoV at an MOI of 0.0001 and incubated at 37°C for 1 h. Serially diluted camostat was then added and incubated with the cells for 18 h. Cells were fixed and stained with crystal violet. Arrow, fused cells. (B) The size of syncytia in the presence or absence of camostat was quantified by counting the number of nuclei in fused cells. Bars and error bars indicate the means and the standard deviations from eight independent syncytia, respectively. ND, syncytia were not detected. (C) Vero-TMPRSS2 cells were infected with MERS-CoV at an MOI of 0.1 and incubated at 37°C for 1 h. Camostat was then added and incubated with the cells for 18 h. Cell lysates and culture media were subjected to SDS-PAGE (7.5% gel and 3 to 10% gel) and Western blot analysis. The viral S protein was detected by using an antipeptide antibody against the VHCR of the MHV-2 S protein, followed by a horseradish peroxidase-conjugated anti-rabbit IgG. GAPDH was employed as the loading control and was detected by using an anti-GAPDH antibody.

L and cathepsin B, these results suggest that MERS-CoV most likely utilizes cathepsin L for cell entry.

Susceptibility of lung-derived cell lines to MERS-CoV. The results presented above were obtained by using artificially constructed Vero cells expressing TMPRSS2. Thus, the following experiments were performed with human lung-derived cell lines (WI-38, MRC-5, and Calu-3 cells). First, the mRNA expression levels of DPP4, TMPRSS2, HAT, cathepsin L, and the lung-specific protein SP-D in total RNA isolated from human lung were quantified using real-time PCR. GAPDH mRNA was used as the internal control, and its expression level was set to a value of 100% (Fig. 7A). Next, the lung-derived cell lines were characterized for their expression levels of transcripts relative to the expression levels in human lung. Susceptible Vero cells and unsusceptible HeLa cells served as the controls.

DPP4 mRNA expression levels were ~10-fold higher in all of the lung-derived cell lines than in human lung, whereas TMPRSS2 mRNA expression levels in Calu-3 cells were similar to those in human lung, but TMPRSS2 mRNA expression was undetectable in MRC-5 and WI-38 cells (Fig. 7B). HAT mRNA expression was also undetectable in all of the cell lines (data not shown), but cathepsin L mRNA expression levels in WI-38, MRC-5, and Calu-3 cells were comparable to those in human lung. SP-D mRNA was detected at low levels in Calu-3 cells and not at all in WI-38 and MRC-5 cells. The results of this analysis suggest that Calu-3 cells most accurately conserve the expression of functional lung proteins required for MERS-CoV entry.

The levels of the human DPP4 protein in the lung-derived cells were also compared by Western blotting. A 100-kDa band corresponding to DPP4 was clearly observed in Calu-3 cells. This band was detected at low levels in WI-38 and MRC-5 cells but was barely detectable in HeLa cells. The DPP4 band was also barely detected in parental Vero cells and Vero-TMPRSS2 cells, which may be due to the fact that Vero cells are derived from the African green monkey, whereas the DPP4 antibody was raised against the human protein.

Next, WI-38, MRC-5, and Calu-3 cells were infected with MERS-CoV, and the effect of protease inhibitors on virus entry was assessed by real-time PCR. Camostat (10 μM) efficiently inhibited virus entry into Calu-3 cells (~10-fold decrease), whereas only slight inhibition was obtained with EST (10 μM) (Fig. 8A). Treatment with camostat plus EST or a single treatment with leupeptin (an inhibitor of cysteine, serine, and threonine peptidases) was no more efficacious than a single treatment with camostat. In addition, virus entry was not significantly blocked by any of the treatments when MRC-5 or WI-38 cells were used instead of Calu-3 cells. Thus, camostat is a powerful agent against MERS-CoV entry into Calu-3 cells. Furthermore, the lack of a pronounced effect with EST suggests that the endosomal virus entry pathway is restricted in Calu-3 cells.

These results also imply that MERS-CoV utilizes proteases other than endosomal cathepsins and cell surface TMPRSS2 for entry into MRC-5 and WI-38 cells. We therefore carefully assessed the inhibitory effects of leupeptin and EST in MRC-5, WI-38, and

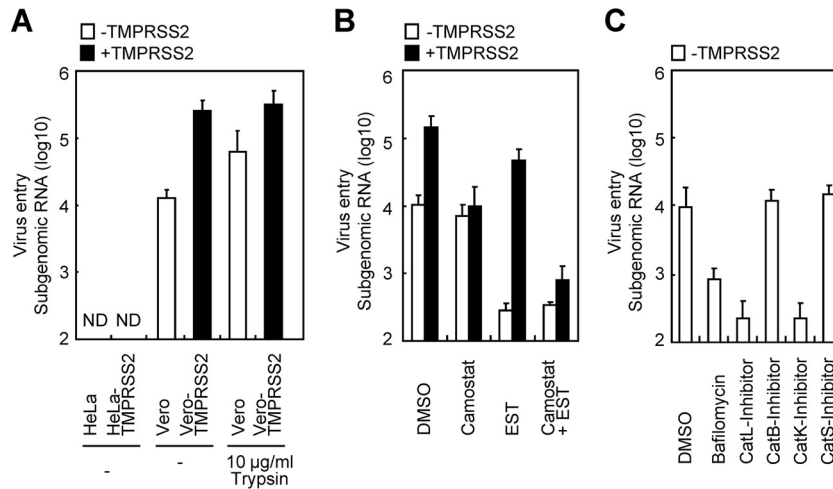


FIG 6 Inhibition of virus entry by treatment with protease inhibitors. (A) Effect of TMPRSS2 expression and exogenous trypsin treatment on virus entry into cells. MERS-CoV was adsorbed onto HeLa, HeLa-TMPRSS2, Vero, or Vero-TMPRSS2 cells for 1 h on ice, followed by the addition of trypsin (1 μ g/ml). Cells were then incubated for a further 5 min at 37°C. The medium was changed, and the cells were incubated for an additional 5 h. (B) Effect of serine and cysteine protease inhibitors on virus entry. Vero or Vero-TMPRSS2 cells were infected with MERS-CoV in the presence of camostat (10 μ M), EST (10 μ M), or camostat plus EST and then incubated for a further 5 h at 37°C. (C) Effect of cathepsin inhibitors or endosome-tropic inhibitors on virus entry. Vero or Vero-TMPRSS2 cells were infected with MERS-CoV in the presence of bafilomycin A1 (100 nM) or inhibitors of cathepsin L (CatL; 10 μ M), cathepsin B (CatB; 10 μ M), cathepsin K (CatK; 10 μ M), or cathepsin S (CatS; 10 μ M). Cells were then incubated for a further 5 h at 37°C. Virus entry was quantified via real-time PCR by using an MERS-CoV-N probe set, as described in Table 1. Dimethyl sulfoxide (DMSO)-treated cells served as the negative control. Bars and error bars indicate the means and the standard deviations from six independent samples, respectively.

Calu-3 cells in a concentration-dependent manner. To facilitate comparison of the decrease in viral infection into MRC-5 and WI-38 cells due to the inhibitors, the data for the control (MERS-CoV entry into Vero and Vero-TMPRSS2 cells in the absence of inhibitors) were assumed to represent 100% viral entry. Figure 8B shows that virus entry was significantly blocked by treatment with leupeptin at concentrations of 10 and 100 μ M in Calu-3 cells, but not in MRC-5 or WI-38 cells. Treatment with EST did not significantly block virus entry into any of the cell lines.

To confirm that endosomal cathepsins and cell surface

TMPRSS2 in MRC-5 and WI-38 cells are not utilized for MERS-CoV entry, an authentic human coronavirus, 229E (HCoV-229E), proficient for infection of MRC-5 and WI-38 cells, was also tested in the virus entry assay in the presence of camostat, EST, or leupeptin. Susceptible HeLa-TMPRSS2 cells were used as the control. Camostat (10 μ M) efficiently inhibited HCoV-229E entry into HeLa-TMPRSS2 cells (7.2-fold decrease), whereas EST (10 μ M) resulted in a 3.0-fold decrease. Camostat and EST together resulted in an 18.3-fold decrease. A much higher concentration of leupeptin is required to inhibit HCoV-229E entry (25); therefore,

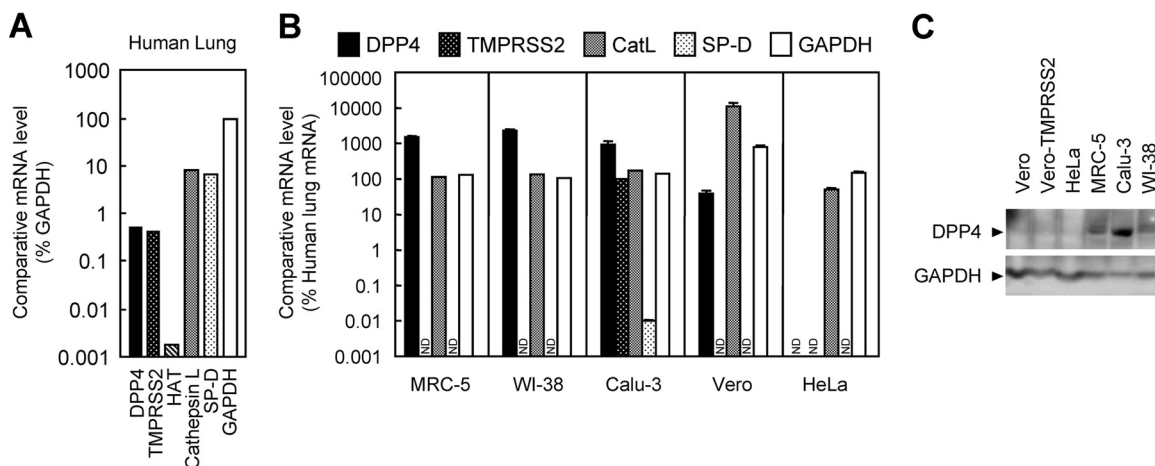


FIG 7 Characterization of human lung-derived cell lines based on the expression of cellular transcripts. (A) DPP4, TMPRSS2, HAT, cathepsin L, SP-D, and GAPDH (loading control) mRNA expression levels were measured in human lungs by using real-time PCR. (B) Total cellular RNA (0.1 μ g) was isolated from WI-38, MRC-5, Calu-3, Vero, and HeLa cells and evaluated for the expression of DPP4, TMPRSS2, cathepsin L (CatL), SP-D, and GAPDH transcripts by using real-time PCR. Expression levels were compared to those in total RNA derived from human lung. ND, transcripts were not detected. (C) Cell lysates were subjected to SDS-PAGE (12.5% gel) and Western blot analysis. DPP4 was detected by using an anti-CD26 antibody, followed by a horseradish peroxidase-conjugated anti-rabbit IgG. GAPDH was employed as the loading control and was detected by using an anti-GAPDH antibody.

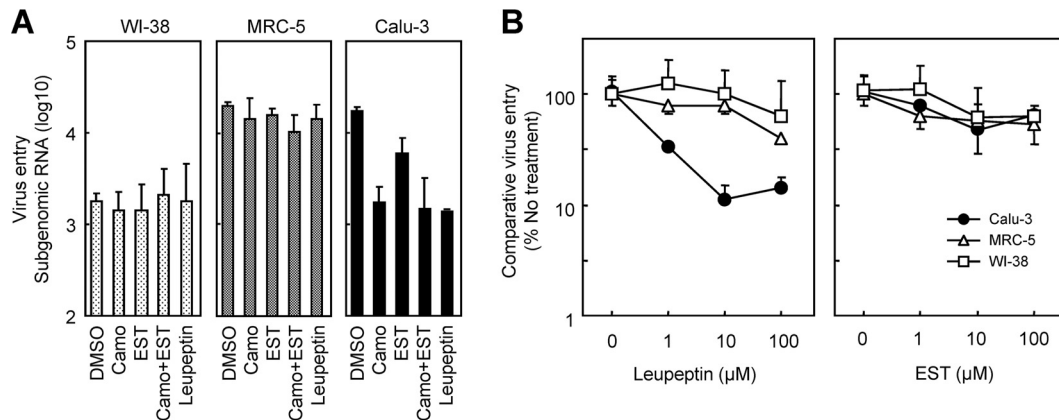


FIG 8 Effect of protease inhibitors on virus entry into human lung-derived cell lines. (A) WI-38, MRC-5, and Calu-3 cells were infected with MERS-CoV in the presence of camostat (Camostat; 10 μ M), EST (10 μ M), camostat plus EST (Camostat+EST), or leupeptin (10 μ M). Cells were then incubated for a further 5 h at 37°C. (B) The concentration-dependent effects of serially diluted leupeptin or EST were tested in the three cell lines. Virus entry was quantified via real-time PCR by using an MERS-CoV-N probe set (Table 1). Dimethyl sulfoxide (DMSO)-treated cells served as the negative control. Bars and error bars indicate the means and the standard deviations from six independent samples, respectively.

100 μ M leupeptin was used, and the result was a 5.4-fold decrease in virus entry. Similar to MERS-CoV entry, HCoV-229E entry into MRC-5 or WI-38 cells was insensitive to inhibition by camostat, EST, or leupeptin (Fig. 9).

Inhibition of multistep virus growth and Calu-3 cell death by camostat. Finally, inhibition of the multistep growth of MERS-CoV and host cell death associated with cell-cell fusion was explored in MRC-5, WI-38, and Calu-3 cells. Cells (10^7) were inoculated with MERS-CoV (10 PFU; MOI = 0.000001) at 37°C for 2 h, washed twice with phosphate-buffered saline, and incubated for 7 days in the presence or absence of camostat. The amount of viral RNA in the culture medium of Calu-3 cells was suppressed by ~90-fold by 10 μ M camostat and by ~270-fold by 100 μ M camostat at 3 days postinfection (Fig. 10A). However, camostat had no significant impact on the amount of viral RNA in the culture medium of the other two cell lines after 3 days (Fig. 10B). Moreover, Calu-3 cell death was delayed by 2 or 5 days by treatment with camostat at a concentration of 10 or 100 μ M, respectively, but WI-38 and MRC-5 cells were not similarly affected. In these cells, 100 μ M camostat partially suppressed cell death, but 10 μ M camostat was not effective (Fig. 10C).

At 7 days postinfection, the level of viral RNA in the culture medium of Calu-3 cells was similar for all conditions, including the highest dose of camostat employed (100 μ M) (Fig. 8A). We assume that camostat activity was lost at 7 days because the drug dose dependently attenuated the recovery of virus levels prior to this time point. For example, virus levels recovered at 4 days with 1 μ M camostat, at 5 to 6 days with 10 μ M camostat, and at 7 days with 100 μ M camostat.

DISCUSSION

The most prominent finding of this study is that large syncytia appeared in Vero-TMPRSS2 cells at only 18 h after MERS-CoV infection. This is in contrast to the findings for SARS-CoV-induced syncytium formation, which took 36 h to occur in our previous study (19). Furthermore, a virus particle-induced cell-cell fusion (i.e., FFWO) was observed at 3 h after MERS-CoV adsorption onto Vero-TMPRSS2 cells, but not after SARS-CoV adsorption. These observations reveal that the MERS-CoV S protein has a high potential for membrane fusion. The molecular mechanism for such robust fusion induction is unclear, but the amount of receptor protein, the affinity of the viral S protein for the cellular receptor, and the intracellular trafficking of the S protein are all likely to be important factors for membrane fusion. Although the effect of cell-cell fusion on viral pathogenicity is also unknown, cell-cell fusion-mediated cytotoxicity may potentially cause the immune system to develop severe inflammation in response to viral infection.

The MERS-CoV was initially isolated by Zaki et al. (1) from a patient in Saudi Arabia. Nevertheless, there have been only five additional reports of virus isolation from other patients. Here, we showed that Vero cells expressing TMPRSS2 are useful for MERS-

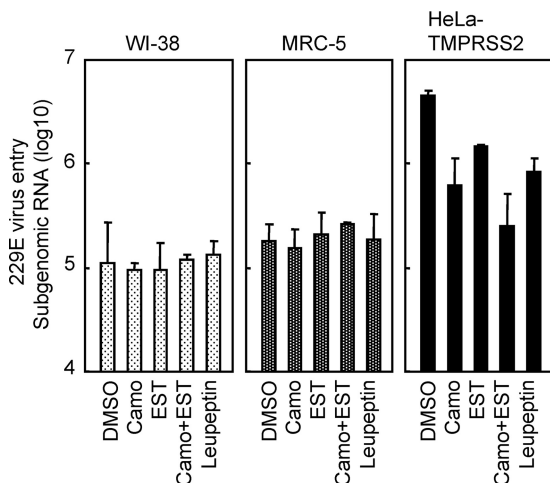


FIG 9 Effect of protease inhibitors on HCoV-229E entry into WI-38 and MRC-5 cell lines. WI-38, MRC-5, and HeLa-TMPRSS2 cells were infected with HCoV-229E in the presence of camostat (Camostat; 10 μ M), EST (10 μ M), camostat plus EST (Camostat+EST), or leupeptin (100 μ M). Cells were then incubated for a further 5 h at 37°C. Virus entry was quantified by real-time PCR by using an HCoV-229E-N probe set (Table 1). Dimethyl sulfoxide (DMSO)-treated cells served as the negative control. Bars and error bars indicate the means and the standard deviations from six independent experiments, respectively.

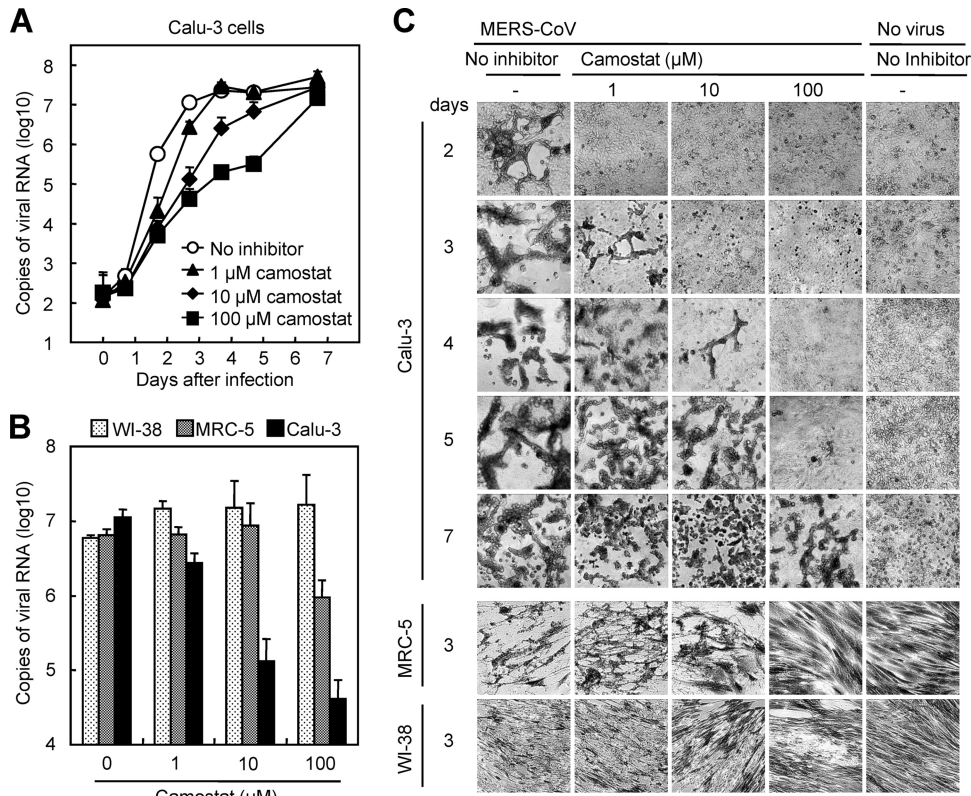


FIG 10 Inhibition of multistep MERS-CoV growth and virus-induced cell death by camostat. (A) Inhibition of multistep virus growth. Calu-3 cells in 24-well plates were infected with MERS-CoV (10 PFU) and incubated in the absence or presence of camostat (1, 10, or 100 μ M). Viral RNA in the culture medium was isolated on the indicated days. (B) Comparison of virus growth among WI-38, MRC-5, and Calu-3 cells in the presence of camostat. Viral RNA in the culture medium was isolated at 3 days after MERS-CoV infection and quantified via real-time PCR by using an MERS-CoV-upE probe set (Table 1). DMSO-treated cells served as the negative control. Bars and error bars indicate the means and the standard deviations from six independent samples, respectively. (C) Inhibition of cytopathic effects by camostat. Calu-3, MRC-5, and WI38 cells were infected with MERS-CoV and treated with camostat as described above, incubated for 3 or 7 days, and observed by phase-contrast microscopy.

CoV detection and isolation because they form large syncytia and are highly susceptible to MERS-CoV infection, both of which can be attributed to the enhancement of virus entry into the cells. Therefore, the use of Vero-TMPRSS2 cells is recommended for MERS-CoV isolation.

We previously reported that TMPRSS2-expressing cells are similar to bronchial epithelial cells in terms of virus entry and susceptibility to SARS-CoV and HCoV-NL63 infection (22). Furthermore, the S protein of SARS-CoV generated in these cells is also intact; that is, the protein is not cleaved by TMPRSS2, because the SARS-CoV S protein is cleaved only following virus binding to the cellular receptor (7, 23). Hence, our current and previous observations signify that cells expressing TMPRSS2 may contribute to virus research and surveillance not only for MERS-CoV but also for other coronaviruses.

Recently, Chan et al. (4) demonstrated the susceptibility to MERS-CoV of various cell lines that span the entire range of MERS-CoV human tissue tropism, which is broader than that of other coronaviruses. Indeed, Müller et al. (26) reported that MERS-CoV can infect primate, porcine, and bat cells, further emphasizing its wide infectivity. Furthermore, DPP4 was identified as the functional receptor for MERS-CoV (5). Although DPP4 is present in the cells of all organs, MERS-CoV is highly pathogenic only in the lungs and the kidney, suggesting that additional factors are required to explain the tropism of this virus.

Gierer et al. (6) determined that pseudotyped MERS-CoV utilizes TMPRSS2 to enter colon-derived Caco-2 cells. In support of this result, the current study showed that authentic MERS-CoV also utilizes TMPRSS2 to enter Vero-TMPRSS2 and Calu-3 cells. Calu-3 cells have a morphology resembling that of nonciliated, pseudostratified columnar epithelial cells, with the expression of microvilli on the apical surface and the formation of tight junction complexes between adjacent cells (27). The mRNA expression levels of TMPRSS2, cathepsin L, and DPP4 were similar in Calu-3 cells and the human lung, implying that Calu-3 cells are similar to human lung cells in terms of their susceptibility to MERS-CoV. A single camostat treatment was as efficacious as leupeptin or EST plus camostat for the blockade of virus entry into Calu-3 cells, suggesting that TMPRSS2 is mainly utilized during virus entry into Calu-3 cells and perhaps into the lung as well. Moreover, the multistep growth of MERS-CoV in Calu-3 cells was significantly inhibited by treatment with camostat, and virus-induced Calu-3 cell death was delayed. Thus, TMPRSS2 or additional serine proteases inhibited by camostat may determine viral tropism and pathogenesis in the lung.

Interestingly, the human fetal fibroblast cell lines MRC-5 and WI-38 are both derived from the human embryonic lung; nonetheless, lung-specific surfactant proteins and TMPRSS2 were not detected in these cells, and neither EST nor leupeptin hindered MERS-CoV infection. These observations imply that MRC-5 and

WI-38 cells differ from mature pneumocytes and that proteases other than cysteine, serine, and threonine proteases may be utilized by MERS-CoV for entry into MRC-5 and WI-38 cells.

ACKNOWLEDGMENTS

We thank Shuetsu Fukushi, Shigeru Morikawa, and Masato Tashiro of the National Institute of Infectious Diseases Japan and Makoto Ujike and Fumihiro Taguchi of the Nippon Veterinary and Life Science University for valuable suggestions and Ron A. M. Fouchier and Bart L. Haagmans of Erasmus Medical Center for providing MERS-CoV.

This work was financially supported by grants from the Ministry of Health, Labor and Welfare of Japan, the Ministry of Education, Culture, Sports, Science and Technology of Japan, and the Astellas Foundation for Research on Metabolic Disorders.

REFERENCES

- Zaki AM, Van Boheemen S, Bestebroer TM, Osterhaus ADME, Fouchier RA. 2012. Isolation of a novel coronavirus from a man with pneumonia in Saudi Arabia. *N. Engl. J. Med.* 367:1814–1820.
- De Groot RJ, Baker SC, Baric RS, Brown CS, Drosten C, Enjuanes L, Fouchier RA, Galiano M, Gorbalenya AE, Memish Z, Perlman S, Poon LL, Snijder EJ, Stephens GM, Woo PC, Zaki AM, Zambon M, Ziebuhr J. 2013. Middle East respiratory syndrome coronavirus (MERS-CoV); announcement of the Coronavirus Study Group. *J. Virol.* 87:7790–7792.
- Danielsson N, ECDC Internal Response Team, Catchpole M. 2012. Novel coronavirus associated with severe respiratory disease: case definition and public health measures. *Euro Surveill.* 17(39):pii=20282. <http://www.eurosurveillance.org/ViewArticle.aspx?ArticleId=20282>.
- Chan JF-W, Chan K-H, Choi GK-Y, To KK-W, Tse H, Cai J-P, Yeung ML, Cheng VC-C, Chen H, Che X-Y, Lau SK-P, Woo PC-Y, Yuen K-Y. 2013. Differential cell line susceptibility to the emerging novel human betacoronavirus 2c EMC/2012: implications for disease pathogenesis and clinical manifestation. *J. Infect. Dis.* 207:1743–1752.
- Raj VS, Mou H, Smits SL, Dekkers DH, Müller MA, Dijkman R, Muth D, Demmers JA, Zaki A, Fouchier RA, Thiel V, Drosten C, Rottier PJ, Osterhaus AD, Bosch BJ, Haagmans BL. 2013. Dipeptidyl peptidase 4 is a functional receptor for the emerging human coronavirus-EMC. *Nature* 495:251–254.
- Gierer S, Bertram S, Kaup F, Wrensch F, Heurich A, Krämer-Kühl A, Welsch K, Winkler M, Meyer B, Drosten C, Dittmer U, Von Hahn T, Simmons G, Hofmann H, Pöhlmann S. 2013. The spike protein of the emerging betacoronavirus EMC uses a novel coronavirus receptor for entry, can be activated by TMPRSS2 and is targeted by neutralizing antibodies. *J. Virol.* 87:5502–5511.
- Simmons G, Reeves JD, Rennekamp AJ, Amberg SM, Piefer AJ, Bates P. 2004. Characterization of severe acute respiratory syndrome-associated coronavirus (SARS-CoV) spike glycoprotein-mediated viral entry. *Proc. Natl. Acad. Sci. U. S. A.* 101:4240–4245.
- Matsuyama S, Taguchi F. 2009. Two-step conformational changes in a coronavirus envelope glycoprotein mediated by receptor binding and proteolysis. *J. Virol.* 83:11133–11141.
- Bertram S, Heurich A, Lavender H, Gierer S, Danisch S, Perin P, Lucas JM, Nelson PS, Pöhlmann S, Soilleux EJ. 2012. Influenza and SARS-coronavirus activating proteases TMPRSS2 and HAT are expressed at multiple sites in human respiratory and gastrointestinal tracts. *PLoS One* 7:e35876. doi:10.1371/journal.pone.0035876.
- Shulla A, Heald-Sargent T, Subramanya G, Zhao J, Perlman S, Gallagher T. 2011. A transmembrane serine protease is linked to the severe acute respiratory syndrome coronavirus receptor and activates virus entry. *J. Virol.* 85:873–882.
- Bertram S, Glowacka I, Blazejewska P, Soilleux E, Allen P, Danisch S, Steffen I, Choi S-Y, Park Y, Schneider H, Schughart K, Pöhlmann S. 2010. TMPRSS2 and TMPRSS4 facilitate trypsin-independent spread of influenza virus in Caco-2 cells. *J. Virol.* 84:10016–10025.
- Bertram S, Glowacka I, Müller MA, Lavender H, Gnirss K, Nehlmeier I, Niemeier D, He Y, Simmons G, Drosten C, Soilleux EJ, Jahn O, Steffen I, Pöhlmann S. 2011. Cleavage and activation of the severe acute respiratory syndrome coronavirus spike protein by human airway trypsin-like protease. *J. Virol.* 85:13363–13372.
- Bertram S, Glowacka I, Steffen I, Kühl A, Pöhlmann S. 2010. Novel insights into proteolytic cleavage of influenza virus hemagglutinin. *Rev. Med. Virol.* 20:298–310.
- Böttcher E, Freuer C, Steinmetzer T, Klenk H-D, Garten W. 2009. MDCK cells that express proteases TMPRSS2 and HAT provide a cell system to propagate influenza viruses in the absence of trypsin and to study cleavage of HA and its inhibition. *Vaccine* 27:6324–6329.
- Böttcher E, Matrosovich T, Beyerle M, Klenk H-D, Garten W, Matrosovich M. 2006. Proteolytic activation of influenza viruses by serine proteases TMPRSS2 and HAT from human airway epithelium. *J. Virol.* 80:9896–9898.
- Böttcher-Friebertshäuser E, Freuer C, Sielaff F, Schmidt S, Eickmann M, Uhlenndorff J, Steinmetzer T, Klenk H-D, Garten W. 2010. Cleavage of influenza virus hemagglutinin by airway proteases TMPRSS2 and HAT differs in subcellular localization and susceptibility to protease inhibitors. *J. Virol.* 84:5605–5614.
- Chaipan C, Kobasa D, Bertram S, Glowacka I, Steffen I, Tsegaye TS, Takeda M, Bugge TH, Kim S, Park Y, Marzi A, Pöhlmann S. 2009. Proteolytic activation of the 1918 influenza virus hemagglutinin. *J. Virol.* 83:3200–3211.
- Choi S-Y, Bertram S, Glowacka I, Park YW, Pöhlmann S. 2009. Type II transmembrane serine proteases in cancer and viral infections. *Trends Mol. Med.* 15:303–312.
- Matsuyama S, Nagata N, Shirato K, Kawase M, Takeda M, Taguchi F. 2010. Efficient activation of the severe acute respiratory syndrome coronavirus spike protein by the transmembrane protease TMPRSS2. *J. Virol.* 84:12658–12664.
- Shirogane Y, Takeda M, Iwasaki M, Ishiguro N, Takeuchi H, Nakatsu Y, Tahara M, Kikuta H, Yanagi Y. 2008. Efficient multiplication of human metapneumovirus in Vero cells expressing the transmembrane serine protease TMPRSS2. *J. Virol.* 82:8942–8946.
- Shirato K, Matsuyama S, Ujike M, Taguchi F. 2011. Role of proteases in the release of porcine epidemic diarrhea virus from infected cells. *J. Virol.* 85:7872–7880.
- Kawase M, Shirato K, Van der Hoek L, Taguchi F, Matsuyama S. 2012. Simultaneous treatment of human bronchial epithelial cells with serine and cysteine protease inhibitors prevents severe acute respiratory syndrome coronavirus entry. *J. Virol.* 86:6537–6545.
- Matsuyama S, Ujike M, Morikawa S, Tashiro M, Taguchi F. 2005. Protease-mediated enhancement of severe acute respiratory syndrome coronavirus infection. *Proc. Natl. Acad. Sci. U. S. A.* 102:12543–12547.
- Saharkhiz-Langroodi A, Holland TC. 1997. Identification of the fusion-from-without determinants of herpes simplex virus type 1 glycoprotein B. *Virology* 227:153–159.
- Kawase M, Shirato K, Matsuyama S, Taguchi F. 2009. Protease-mediated entry via the endosome of human coronavirus 229E. *J. Virol.* 83:712–721.
- Müller MA, Raj VS, Muth D, Meyer B, Kallies S, Smits SL, Wollny R, Bestebroer TM, Specht S, Suliman T, Zimmermann K, Binger T, Eckerle I, Tschapka M, Zaki AM, Osterhaus AD, Fouchier RA, Haagmans BL, Drosten C. 2012. Human coronavirus EMC does not require the SARS-coronavirus receptor and maintains broad replicative capability in mammalian cell lines. *mBio* 3(6):e00515–12. doi:10.1128/mBio.00515-12.
- Yoshikawa T, Hill TE, Yoshikawa N, Popov VL, Galindo CL, Garner HR, Peters CJ, Tseng C-TK. 2010. Dynamic innate immune responses of human bronchial epithelial cells to severe acute respiratory syndrome-associated coronavirus infection. *PLoS One* 5:e8729. doi:10.1371/journal.pone.0008729.